Temperature gradient-driven motion of magnetic domains in a magnetic metal multilayer: Supplementary material

Lin Huang,[1,2,*] Joseph Barker,[1] Lekshmi Kailas,[1] Soumyarup Hait,[1]
Simon D. Connell,[1] Gavin Burnell,[1] and Christopher H. Marrows[1,†]

[1] *School of Physics and Astronomy, University of Leeds, Leeds LS2 9JT, United Kingdom.*
[2] *School of Material Science, University of Sheffield, Sheffield S10 2TN, United Kingdom.*

S.1. SAMPLE PATTERNING, CALIBRATION OF PLATINUM HEATER/THERMOMETER, AND IMAGING

The current contacts were Ti (5 nm)/Au (100 nm) bilayers, deposited by thermal evaporation, which were patterned by photolithography. The bilayer photoresists were S1813 (spin coated at 300 rpm and baked for 180 s on a 185°C hot plate) and LOR3B (spin coated at 3000 rpm and baked for 60 s on a 115°C hot plate).

To generate the temperature gradient along the magnetic track, a dc current was passed through the Pt heater in order to heat the magnetic track at the point where the track and heater cross. The dc current for heater was injected with a Keithley 6221 current source. To perform the calibration of the Pt thermometer/heater resistance, the ac resistance of the Pt heater was measured using a SR830 lock-in amplifier, with the ac sense current also supplied by the Keithley 6221. The 'K' shape of the Pt heater means that we could make a four-point resistance measurement for thermometry at that point. We measured the temperature coefficient of resistance of the Pt wire and then used the measured steady-state resistance rise for a given dc current to generate the calibration curve shown in Fig. S**??**. The laboratory temperature, and hence the ambient temperature of the magnetic track far from the heater, was around 290 K.

The samples were imaged by atomic (AFM) and magnetic force microscopy (MFM) using an Asylum Research MFP-3D microscope, using ASYLMFLC-R2 magnetic coated MFM tips. Out-of-plane magnetic fields were applied by means of a Variable Field Module VFM3, which uses permanent magnets and so avoids any inadvertent sample heating.

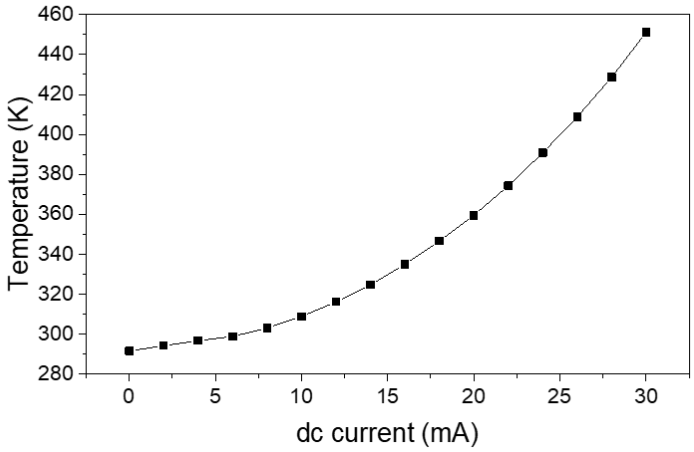

Figure S1. Temperature reached by Pt heater as a function of heater current.

* Present address: University of Southampton, CORNERSTONE, Optoelectronics Research Centre (ORC), Building 60, University Road, Southampton SO17 1BJ, United Kingdom.
† Email: c.h.marrows@leeds.ac.uk

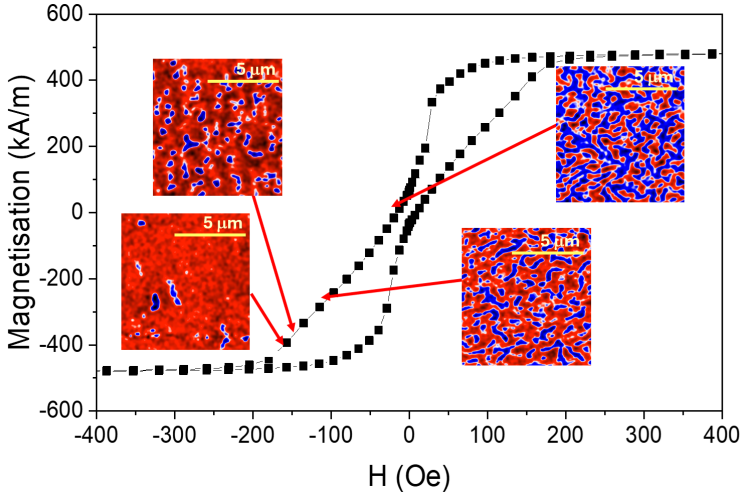

Figure S2. Hysteresis loop under out-of-plane field for a sheet film Ta(20 Å)/[Pt(7 Å)/$Co_{68}B_{32}$(8 Å)/Ir(5 Å)]$_{\times 10}$/Pt(14 Å) multilayer subjected to the same heating processes that occur during track fabrication. False colour MFM images show the magnetic domain patterns for selected positions on the loop, indicated by the red arrows.

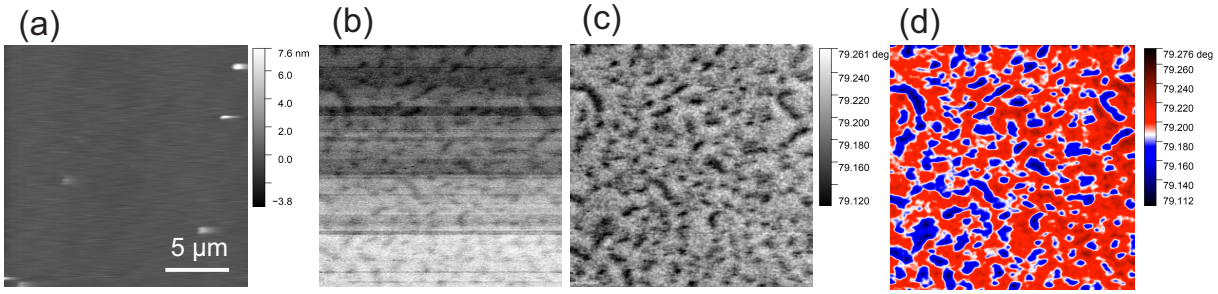

Figure S3. An example of the MFM image processing workflow, for an image acquired at -135 Oe. This is an additional image from the hysteresis loop shown in Fig. S**??**. (a) Height image, (b) raw MFM image ('NapPhaseRetrace') acquired on Asylum Research MFP-3D equipped with a Variable Field Module VFM3. (c) Gray scale MFM image line-levelled to 0^{th} order (no masking) and contrast enhanced. (d) Final image is smoothed with a 1 pixel width Gaussian filter in Gwyddion, and a blue-red color palette applied.

S.2. SHEET FILM HYSTERESIS CURVE

In Fig. S**??**, we show an out-of-plane hysteresis loop measured by SQUID-vibrating sample magnetometry for a sheet film of multilayer subjected to the same heating processes that occur during track fabrication. Its low saturation field shows that there is preferentially perpendicular magnetisation that reverses through domain formation processes. Some of the associated domain structures at selected values of field, observed by magnetic force microscopy (MFM), are shown as insets.

At the coercive field, which is also close to remanence, the sample is equally divided into up and down domains with an interconnected labyrinthine appearance. As the reverse field is made stronger, the forward-magnetized domains become discrete objects, some with a circular form, others with an extended worm-like appearance. These become fewer and fewer in number until approaching the saturation magnetic field where only a few remain. Even at this point, where the temperature gradient-driven motion experiments were carried out, many domains still have an extended appearance.

S.3. MFM IMAGE PROCESSING

In Fig. S**??** we show the workflow used for MFM image processing, which was carried out in part by using the Gwyddion software package [**?**]. The process involved, line-levelling, contrast enhancement, and smoothing, before a blue-red color palette is applied.

S.4. GAUSSIAN FITTING

The positions and widths of the Gaussians fitted to the dips in contrast in the line profiles shown in Fig. 1(g) of the main text, before and after the application of the −30 mA current, are given in Table **??**. Contrast dips are either labelled as defects 'd' when occupying positions identified in the MFM image under a saturating field in Fig. 1(b), or domains 'D' when motion is detected.

For the contrast dips that are pure defects (d1, d2, and d5), no motion of the fitted Gaussian centre is detected within the uncertainty of the fits. Domains D1 and D3 are found away from the defect positions and the motion of the fitted gaussian centre is clearly the motion of the domain itself. In some cases (d3+D2 and d4+D4) we have a contrast dip that is at a position where a defect was identified but we also see motion of the fitted gaussian centre. We take these to be domains that have (not unexpectedly) nucleated at defects and have been subjected to driving forces arising from the temperature gradient that have caused their positions to shift.

S.5. EFFECTS OF HEATER-GENERATED OERSTED FIELDS

A current in the heater wire will give rise to both heating and an Oersted field, both of which decay with distance along the track from the heater wire position. We consider how the Oersted field gradient will affect magnetic textures in the track in combination with the temperature gradient.

Taking the first case shown in Fig. S**??** (a), the wire is preferentially magnetized by a vertical upwards externally applied field H (blue) but still contains some reverse domains (red). For a positive dc current I in the heater (yellow) the moment in these domains opposes the circulating Oersted field, and so the seeks a weaker Oersted field, which is further from the wire. Hence the Oersted field gradient generates a repulsive force on the domain $F_{\text{repulsion}}$, which opposes the thermal force F_{Heat} if we assume that that force causes the domain to move toward the hot end of the gradient.

Reversing both the sense of both H and I will still lead to a repulsive force from the Oersted field gradient. Reversing only one or the other will give rise to an attractive force Oersted field force $F_{\text{attraction}}$, Fig. S**??**(b), which enhances the force from the temperature gradient F_{Heat}.

Hence, this picture is consistent with our experimental observation that the domain motion is always towards the heater, but varies depending on the relative alignment of the heater current direction and magnetisation within the domains.

TABLE I. Gaussian fitting results for the contrast dips in the line profiles along the magnetic track shown in Fig. 1(g). These correspond to before (profiles 1 and 3) and after (profiles 2 and 4) application of a -30 mA heater current I for two minutes at two different positions across the track width

Line Profile (colour)	Feature	Application of current	Gaussian width (nm)	Gaussian centre (nm)
1 (Black)	defect d1	before	390 ± 30	330 ± 10
2 (Orange)	defect d1	after	390 ± 20	330 ± 10
1 (Black)	domain D1	before	130 ± 10	1840 ± 10
2 (Orange)	domain D1	after	200 ± 20	1720 ± 30
1 (Black)	defect d2	before	180 ± 20	2370 ± 10
2 (Orange)	defect d2	after	160 ± 10	2370 ± 10
3 (Blue)	defect d3 + domain D2	before	400 ± 10	310 ± 20
4 (Pink)	defect d3 + domain D2	after	270 ± 20	230 ± 10
3 (Blue)	domain D3	before	150 ± 10	1270 ± 10
4 (Pink)	domain D3	after	150 ± 40	1200 ± 10
3 (Blue)	defect d4 + domain D4	before	160 ± 20	2420 ± 10
4 (Pink)	defect d4 + domain D4	after	220 ± 20	2390 ± 10
3 (Blue)	defect d5	before	200 ± 20	3070 ± 20
4 (Pink)	defect d5	after	350 ± 20	3090 ± 40

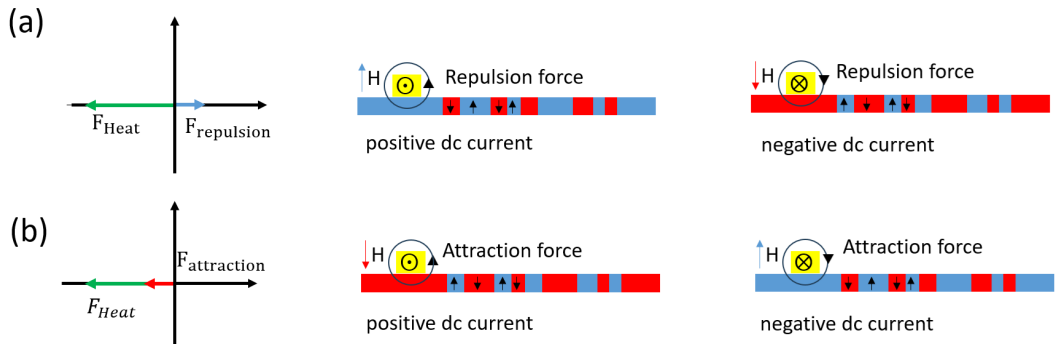

Figure S4. Forces on reverse domains considered in a side view of the track. Heater currents flow into or out of the plane of the paper. (a) A repulsive force on reverse domains can be generated by the Oersted field gradient when the Oersted field direction in the track matches the externally applied field (H) direction. (b) An attractive force on reverse domains can be generated by the Oersted field gradient when the Oersted field direction in the track opposes the externally applied field (H) direction.

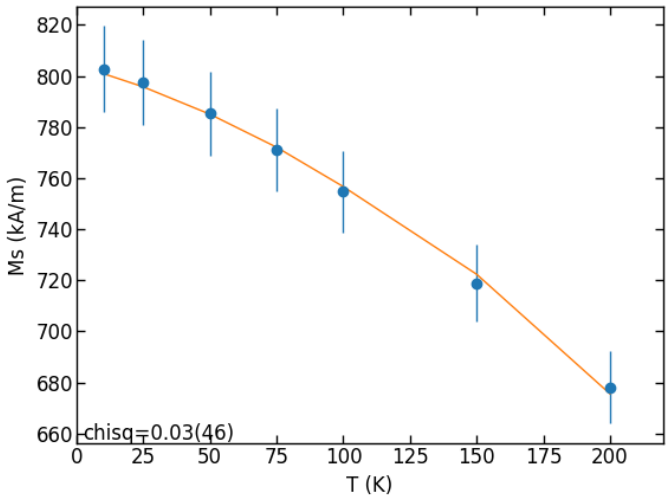

Figure S5. Fitting Eq. (S**??**), thin film Bloch's law, to the experimentally measured magnetisation. Blue points are the experimental measurements and their error bars. The orange curve is Eq. (S**??**) with the best fit parameters $D_0 = (5.65^{+1.25}_{-0.55}) \times 10^{-40}$ Jm^2 and $M_0 = (803.33^{+7.27}_{-11.33})$ kA/m.

S.6. FITTING BLOCH'S LAW

The form of the Bloch law for a thin film was given in the main text as

$$M_s(T) = M_0 + \frac{\gamma\hbar}{4\pi L_z}\frac{k_B T}{D_0}\sum_{m=0}^{N-1} \ln\left[1 - \exp\left(-\frac{\omega_m}{k_B T}\right)\right]. \tag{S1}$$

We fitted Eq. (S**??**) to the experimental data from the lowest temperature up to $T = 200$ K. For B_z we used the in-plane saturation field from the hysteresis loop at each temperature as a measure of the coercive field of the film. i.e. $B_z \to B_z(T)$. We fit using the DREAM Markov chain Monte Carlo algorithm as implemented in the BUMPS package [**?**]. The settings are burn = 1000, samples = 10^6, init = eps. The full fitting script and results are available in the data upload. The best fit gives $D_0 = (5.65^{+1.25}_{-0.55}) \times 10^{-40}$ Jm^2 and $M_0 = (803.33^{+7.27}_{-11.33})$ kA/m where the errors represent the 68% confidence interval.